Improved space charge suppression in PP/SEBS nanocomposites by controlling MgO nanoparticles with abundant surface defects

Qi Cheng[1,2], Jun-Wei Zha[1,2,3,a)*], Jin-Tao Zhai[2], Dong-Li Zhang[1], Xingming Bian[3], George Chen[4], and Zhi-Min Dang[1,a)*]

[1]*State Key Laboratory of Power System, Department of Electrical Engineering, Tsinghua University, Beijing 100084, P. R. China*

[2]*School of Chemistry and Biological Engineering, University of Science and Technology Beijing, Beijing 100083, P. R. China*

[3]*State Key Laboratory of Alternate Electrical Power System with Renewable Energy Sources, North China Electric Power University, Beijing 102206, P. R. China*

[4]*Department of Electronics and Computer Science, University of Southampton, Southampton SO17 1BJ, United Kingdom*

Abstract: Polymer nanocomposite dielectrics have received extensive attention in the field of electrical materials and equipment. Studies have shown that the interface region between the nanoparticles and polymer matrix has an important influence on the properties of nanocomposites. In this paper, MgO nanoparticles with abundant surface defects (C-MgO) containing a highly effective interface is synthesized by surface carbonization. A ternary nanocomposite is prepared by melt blending with polypropylene (PP) and styrene-(ethylene-co-butylene)-styrene tri-block copolymer (SEBS). The results showed that size of the prepared concave nanoparticles was around 100 nm. The addition of 0.2 phr of C-MgO had the smallest charge accumulation in the PP/SEBS/C-MgO nanocomposites, which greatly reduced the electric field distortion and enhanced the charge release ability. Moreover, the DC breakdown strength was increased to 304 kV/mm, may be due to the introduction of nanoparticles with high surface vacancy defects which provided deep traps. In addition, C-MgO nanoparticles increased the dielectric permittivity. The tensile strength

*Authors to whom correspondence should be addressed: E-mail: zhajw@ustb.edu.cn, dangzm@tsinghua.edu.cn

and elongation at break of PP/SEBS/C-MgO composites were significantly increased, due to the rugged structure of the particles which acted as dispersion stress centers in the polymer matrix. This work helps to develop environmental polymer nanocomposites and promotes the development and application of flexible HVDC technology.

Keywords: Dielectric property, space charge, HVDC cable, polypropylene, nanocomposites

Cross-linked polyethylene (XLPE) has been used for many years as an insulating material for high-voltage direct-current (HVDC) transmission systems. XLPE is the most popular material owing to its superior electrical and mechanical properties in HVDC cables. However, the traditional XLPE is gradually becoming a thorny issue as it is a thermoset material that is not easily recyclable. In general, common XLPE cables are treated by incineration, which leads to environmental pollution and waste material disposal.[1-4] Polypropylene (PP) has excellent mechanical and dielectric properties and is known as a material with superb heat and chemical resistances, high stiffness, and great heat distortion temperature. Furthermore, PP shows good recycling properties and can be applied as a potent eco-friendly material in advanced HVDC cables. Polypropylene is also a high-melting material and shows excellent electrical insulating properties.[5-7] However, the brittleness of polypropylene at normal temperatures limited its direct application as a cable insulation material in HVDC cables. In order to solve the above drawbacks, elastomers are often introduced to improve the mechanical properties of PP. In addition, the issue of space charge in the insulation has been one of the most important challenges in the development of plastic insulated cables. The low conductivity of a polymeric material causes difficult diffusion of the accumulated internal space charge. Therefore, serious local electric field distortion may occur, especially when

there is a temperature gradient effect during full load operation, which drastically reduces their service lifetime.[8-13]

In recent years, it has been found that nanoparticles have excellent performance to improve the properties of polymer materials, because of their quantum size effect and large specific surface area.[14,15] Since the concept of nano-dielectrics has been proposed by T. J. Lewis in 1994,[16] scholars have conducted extensive research on the performance and mechanism of improvements achieved in the polymeric insulating materials after addition of nanoparticles.[17,18] Depending on the particle size, shape, and doping amount of the nanoparticles, the polymer matrix shows different nano-dielectric behaviors. Therefore, various levels of space charge inhibition, dielectric properties, heat performance, and enhanced mechanical properties can be achieved by insertion of nanoparticles into the polymer matrix.

Polymer nanocomposites incorporated with different nanosized inorganic fillers such as MgO, ZnO, Al_2O_3, SiO_2, etc., are applied as HVDC cable materials. These stuffs effectively suppress the space-charge accumulation, significantly improve insulating and mechanical properties, and induce high thermal stability to the mentioned manufactures.[19-23] The interface between the particles and matrix helps the carriers to be trapped by the interfacial traps between the nanomaterial and polymer during the transition process and, eventually, limits the migration of electrons and holes. T. Takada proposed a multi-core model and interface model to reveal the mechanism of that action.[24] Extensive researches have been carried out to improve interface compatibility. In the present study, synthesis of highly effective interface nanoparticles incorporated into the polymer matrix is disclosed to suppress the space charge.

In this letter, MgO nanoparticles bearing abundant surface defects (C-MgO) were prepared as shown in Fig. 1(a) (see supporting information for the detailed procedure of sample preparation).

Morphologies of C-MgO were observed through transmission electron microscope (TEM, SU8010, Hitachi, Japan) and scanning electron microscopy (SEM, S4700 Hitachi, Japan). Fig. 1(b) shows the TEM image of C-MgO describing an uneven state outline for the nanoparticles. The surface of the nanoparticles had a depression and the particle size was about 100 nm as shown in Fig. S1 (see supporting information). This depression would be a surface vacancy defect caused by the participation of carbon dioxide. The prepared MgO nanoparticles were rich in low coordination surface defects of O_3C^{2-} , which can generate energy levels in the band gap of the MgO nanoparticles. The formation of defects induced a certain impact on the performance of the composites. X-ray diffraction patterns of C-MgO nanoparticles are shown in Fig. S2 (see supporting information). The characteristic peaks with the 2θ values of 36.9°, 42.9°, 62.3°, 74.6° and 78.6° are corresponded to the (111), (200), (220), (311), and (222) planes of MgO crystal, respectively. It can be seen that the peaks are relatively sharp, have no miscellaneous peak, and each diffraction peak is consistent with the standard PDF card (JCPDS: 04-0829). It indicated that the impurity removal has been sufficient during the synthesis route to obtain a highly pure MgO.

The prepared environment-friendly materials are highly effective insulators which are composed of isotactic PP, styrene-(ethylene-co-butylene)-styrene tri-block copolymer (SEBS) and C-MgO nanoparticles. The content of C-MgO was 0, 0.2, 0.4, 0.7 and 1.0 phr, respectively (where 1.0 phr indicates 1 g of C-MgO nanoparticles in 100 g of PP/SEBS blends). Fig. 2 shows the SEM cross-sectional images of PP/SEBS/C-MgO nanocomposites. As Fig. 2(b) shows, when the content of C-MgO in the composite material was 0.2 phr, almost no agglomeration occurred, and the dispersion of C-MgO was relatively uniform. However, when the C-MgO content reached to 0.7 and 1.0 phr, the agglomeration between C-MgO particles was very serious, as shown in Figs. 2(d)

and 2(e). In contrast, when 0.2 phr of C-MgO was added, the distribution of nanoparticles in the composite was optimal.

In general, differential scanning calorimetry (DSC) is mainly used to describe the crystallization process of some blends to get information about the melting point and crystallinity of a material. X_c is related to the enthalpy of melting (ΔH_f) and can be calculated by Eq. (1).

$$X_c = \frac{\Delta H_f}{\Delta H_c} \times 100\% \qquad (1)$$

where ΔH_c is the melting enthalpy under the complete crystallization about 165 J/g. Fig. 3 shows the melting curve of PP/SEBS/C-MgO nanocomposite. The crystallinity (X_c) of the material was obtained by Eq. (1) and the crystallinity of 37-50% was attained. With the incorporation of C-MgO nanoparticles, the crystallinity of the composite first decreased and then increased as shown in Table S1 (see Supporting information). Due to the low content of nanoparticles, spherulite-growth dominated, and the strong interfacial interaction between the nanoparticles and polymer matrix hindered the movement of the segments which are required for the crystal-growth of the polymer. Therefore, the crystallization activation energy was increased as the content of the nanoparticles enhanced. However, after increasing to a certain amount, the activation energy of the polymer crystal began to decrease slowly. As shown in Table S1, the melting peak of the composite material was almost about 162 ^{o}C, indicating that the added C-MgO and SEBS had little effects on the melting point of PP. This is mainly due to the good compatibility of the polymer matrix with the nanoparticles. Doping of the nanoparticles caused alteration of the chain-entanglement density of the polymer molecules; thus, the molecular chain motions were changed and the crystallinity and melting point of the polymer were modified.

Space charge distribution was measured using the pulsed electro-acoustic (PEA) method at room temperature. Fig. 4 shows the space charge distribution in the nanocomposites with different contents of C-MgO at 60 kV/mm for 90 min. As shown in Fig. 4(a), the introduction of SEBS produced a large amount of heteropolar space charge across the electrode. Compared to Fig. 4(a), there is almost no accumulation of the heteropolar charges at both ends of the electrode in Fig. 4(b), which means that 0.2 phr of C-MgO can substantially suppress the injection and accumulation of the space charge. Studies have shown that nanoparticles can introduce traps into the polymer matrix, effectively bind the charges, and inhibit space charge accumulation. However, the content of the nanoparticles directly influences concentration of the trap, so that high trap concentration reduces the electrical properties of the material. In fact, as the content of C-MgO was increased, the accumulation of space charge was appeared again as shown in Figs. 4(c)-4(d).

Fig. 5 describes the corresponding electric field distortion of PP/SEBS/C-MgO nanocomposites. The electric field distortions were 7.7, 3.0, 6.8, 6.9, and 6.7 kV/mm, respectively, and the variation of space charge was consistent. The space charge accumulation was suppressed in the presence of 0.2 phr doping with C-MgO nanoparticles, and the electric field distortion was minimized. However, when the content of C-MgO was increased again, the electric field distortion was grown. This phenomenon is likely to be due to the incorporation of traps when C-MgO is added to the PP/SEBS matrix. The trap captured the carriers and reduced the migration of carriers inside the material. However, when the content of C-MgO nanoparticles was high, the carriers could easily transit between the adjacent traps through tunneling, forming a passage for easy transfer of carriers. Therefore, the space charge accumulation was remarkably increased and the corresponding electric field distortion became severe again. Fig. S3 displays the dissipation curve of the charge when PP/SEBS/C-MgO nanocomposites were depolarized after 90 min of pressurization.

As can be seen from Fig. S3, the charge inside the material dissipated rapidly, indicating that the charge was more likely to migrate from the inside to the outside during the short circuit. When the nanocomposite with 0.2 phr of C-MgO was short-circuited for 1200 s, the internal charge of the material was almost zero near the cathode.

The breakdown strength was evaluated by the Weibull analysis according to Eq. (2) as follows:

$$P = 1 - \exp\left[-\left(\frac{E}{\alpha}\right)^{\beta}\right] \tag{2}$$

where P is the failure probability, E is the measured electrical breakdown strength, α is nominal field which corresponding to 63.2% cumulative probability of dielectric breakdown and β is the shape factor which reflect the distribution of data (the higher value of β means the lower scattering). The thicknesses of PP/SEBS/C-MgO nanocomposites used are all about 150 μm. When the content of C-MgO nanoparticles was 0 phr, 0.2 phr, 0.4 phr, 0.7 phr, and 1.0 phr, the breakdown strengths were, respectively, 289, 304, 291, 284, and 283 kV/mm, which shows an enhancement at first and then a clear decrease as shown in Fig. 6a. This result coincides with the conclusions obtained from the above space charge. Most of the traps in PP/SEBS are shallow traps, and charges can migrate freely. When C-MgO nanoparticles were added to the matrix with a gradual increase in the content, a certain number of deep traps were introduced at the interface. The contact of the carrier with the electrode was changed from the ohmic contact to the barrier contact, and movement of the charge was limited, thus the DC breakdown strength was improved. However, when the trap density was too high, the relative distance between the traps was relatively small, and the carrier was easily transmitted by the electron tunneling effect. Thus, the DC breakdown field strength was lowered again just as a free conductive path was formed.

Dielectric properties of the nanocomposites were tested by a precision impedance analyzer (Agilent 4294A) within the frequency range of 10^2 to 10^6 Hz. Figs. 6(b) and 6(c) correlates the frequency with the dielectric properties of PP/SEBS/C-MgO nanocomposites at room temperature. Fig. 6(b) shows that by increasing of the filler content in PP/SEBS/C-MgO nanocomposites, the dielectric permittivities of 2.7, 3.1, 2.9, 2.8, and 2.9 were attained in the frequency range of 10^3-10^6 Hz. The highest dielectric permittivity was observed when the content of PP/SEBS/C-MgO was 0.2 phr. The dielectric loss of PP/SEBS/C-MgO nanocomposites is shown in Fig. 6(c). Obviously, the dielectric loss had been slightly increased by the addition of C-MgO, but the overall value of the dielectric loss of the material was still very small. Meanwhile, the dielectric loss of PP/SEBS/C-MgO nanocomposites decreases with increasing frequency. This is because that at low frequencies, the sample undergoes electronic displacement polarization, ion displacement polarization and space charge polarization, resulting in a larger dielectric loss. As the frequency increases, the space charge polarization gradually decreases, thereby reducing the dielectric loss of the sample.

The low elongation of PP at break confirms low temperature brittleness of this material. The elongation at break of nanocomposite involving C-MgO was more than 800%, indicating that the surface carbonized uneven particle structure played an important role in dispersing stress in the polymer matrix and synergistic toughening. Both the tensile strength and elongation at break of the nanocomposite were increased after the addition of C-MgO nanoparticles, as shown in Fig. S4 (see supporting information). This observation was due to the fact that the added particles were distributed in the matrix and formed a local resistance strain. The stress was transmitted between the nanoparticles, thereby, the distribution state of the stress in the composite material was changed.

Therefore, the tensile strength was increased and a good toughening effect and improved mechanical properties were attained by increasing the binding force with the matrix.

In summary, C-MgO nanoparticles with abundant surface defects were synthesized and a ternary nanocomposite was prepared through melt blending with PP and SEBS. When the content of C-MgO nanoparticles was 0.2 phr, the filler was well dispersed in the matrix. The space charge was significantly suppressed, the breakdown strength was increased to 304 kV/mm, and the largest dielectric constant was attained. In addition, the elongation at break of the nanocomposite involving C-MgO was higher than 800%, indicating that the surface carbonized uneven particle structure and the polymer matrix had a synergistic toughening effect. These results provided a reference for further research on the performance of added nanoparticles to control polypropylene and achieved a meaningful progress to the development of recyclable and environmental DC cable insulation materials.

See supporting information for the detailed procedure of sample preparation, morphology and XRD patterns of C-MgO nanoparticles, charge decay distribution and mechanical properties of PP/SEBS/C-MgO nanocomposites.

Acknowledgment

This work was financially supported by National Nature Science Foundation of China (No. 51622701, 51425201), National Basic Research Program of China (973 Program, 2014CB239501), Beijing Nova Program (Z181100006218006), Fundamental Research Funds for the Central Universities (No. FRF-TP-16-001C1), and the State Key Laboratory of Alternate Electrical Power System with Renewable Energy Sources (Grant No. LAPS19001).

References

[1]M. Jarvid, A. Johansson, R. Kroon, J. M. Bjuggren, H. Wutzel, V. Englund, S. Gubanski, M. R. Andersson, C. Müller, Adv. Mater. **27**, 897 (2015).

[2]J. Fothergill, G. Montanari, G. Stevens, C. Laurent, G. Teyssedre, L. Dissado, U. Nilsson, G. Platbrood, IEEE Trans. Dielectr. Electr. Insul. **10**, 514 (2003).

[3]Y. H. Wu, J. W. Zha, W. K. Li, S. J. Wang, Z. M. Dang, Appl. Phys. Lett. **107,** 112901 (2015).

[4]X. Zheng, G. Chen, IEEE Trans. Dielectr. Electr. Insul. **15**, 800 (2008).

[5]B. Lotz, J. C. Wittmann, A. J. Lovinger, Polymer 37 (1996) 4979-4992.

[6]J. W. Zha, H. D. Yan, W. K. Li, Z. M. Dang, Appl. Phys. Lett. **109**, 222902 (2016).

[7]I. L. Hosier, A. S. Vaughan, S. G. Swingler, J. Mater. Sci. **45**, 2747 (2010).

[8]Y. Zhou, J. L. He, J. Hu, B. Dang, J. Appl. Polym. Sci. **133**, 42863 (2016).

[9]J. Li, H. C. Liang, B. X. Du, Z. H. Wang, IEEE Trans. Electr. Insul. **26**, 664 (2019).

[10]S. J. Wang, J. W. Zha, W. K. Li, Y. Wang, Y. Q. Wen, G. Chen, Z. M. Dang, Compo. Sci. Technol. **135**, 100 (2016).

[11]B. Ohlsson, B. Törnell, Polym. Eng. Sci. **36**, 1547 (1996).

[12]G. Wu, Y. Wang, K. Wang, A. Feng, RSC Adv. **6**, 102542 (2016).

[13]J.H. Gao, D. Xue, L. Zhang, Y. Wang, H. Bao, C. Zhou, W. Liu, W. Chen, X. Ren, Euro. Phys. Lett. **96**, 370 (2011).

[14]D. R. Paul, L. M. Robeson, Polymer **49**, 3187 (2008).

[15]N. Guo, S. A. DiBenedetto, P. Tewari, M. T. Lanagan, M. A. Ratner, T. J. Marks, Chem. Mater. **22**, 1567 (2010) .

[16]T. J. Lewis, IEEE Trans. Electr. Insul. **1**, 812 (1994).

[17]L. K. H. Pallon, R. T. Olsson, D. Liu, A. M. Pourrahimi, M. S. Hedenqvist, A. T. Hoang, S. Gubanski, U. W. Gedde, J. Mater. Chem. A **3**, 7523 (2015) .

[18]J. W. Zha, Y. Wang, W. K. Li, S. J. Wang, Z. M. Dang, IEEE Trans. Electr. Insul. **24,** 1457 (2017).

[19]A. M. Pourrahimi, T. A. Hoang, D. M. Liu, L. K. H. Pallon, S. Gubanski, R. T. Olsson, U. W. Gedde, M. S. Hedenqvist, Adv. Mater. **28**, 8651 (2016).

[20]S. P. Fillery, H. Koerner, L. Drummy, E. Dunkerley, M. F. Durstock, D. F. Schmidt, R. A. Vaia, ACS Appl. Mater. Interfaces **4**, 1388 (2012).

[21]X. Yang, Y. Guo, X. Luo, N. Zheng, T. Ma, J. Tan, C. Li, Q. Zhang, J. Gu. Compo. Sci. Technol. **164**, 59 (2018).

[22]T. Krentz, M. M. Khani, M. Bell, B. C. Benicewicz, J. K. Nelson, S. Zhao, H. Hillborg, L. S. Schadler, J. Appl. Polym. Sci. **134**, 44347 (2017).

[23]I. N. Hidayah, M. Mariatti, H. Ismail, M. Kamarol, Plastics, Rubber Compo. **44**, 259 (2015).

[24]T. Tanaka, M. Kozako, N. Fuse, Y. Ohki, IEEE Trans. Dielectr. Electr. Insul. **12**, 669 (2005).

Figure captions

FIG. 1. (a) Schematic illustration of the preparation of MgO nanoparticles via carbonization method, (b) TEM images of C-MgO nanoparticles

FIG. 2. SEM images of PP/SEBS/C-MgO nanocomposites with different contents of C-MgO (a) 0, (b) 0.2, (c) 0.4, (d) 0.7 and (e) 1.0 phr of C-MgO.

FIG. 3. DSC curves of the PP/SEBS/C-MgO nanocomposites.

FIG. 4. Space charge distribution in PP/SEBS/C-MgO nanocomposites with different contents of C-MgO under the applied electric field of 60 kV/mm: (a) 0, (b) 0.2, (c) 0.4, (d) 0.7, and (e)1.0 phr of C-MgO.

FIG. 5. Electrical field distribution of PP/SEBS/C-MgO nanocomposites with different contents of C-MgO under the applied electric field of 60 kV/mm for 90 min.: (a) 0, (b) 0.2, (c) 0.4, (d) 0.7, and (e) 1.0 phr of C-MgO.

FIG. 6. (a) Weibull-distribution plot of the breakdown field strength of PP/SEBS/C-MgO nanocomposites. Frequency dependence of (b) dielectric permittivity and (c) dielectric loss tangent of PP/SEBS/C-MgO nanocomposites with different C-MgO contents.

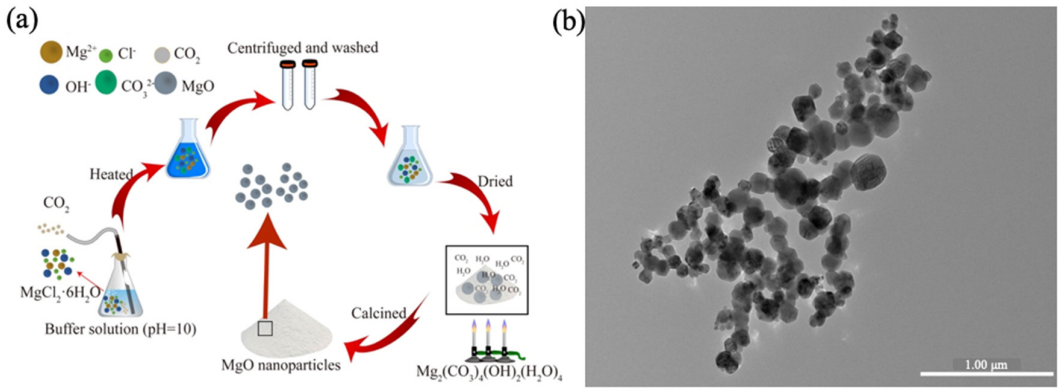
(a)
Mg2+
Cl-
CO2
OH-
CO3 2-
MgO
Centrifuged and washed
Heated
Dried
CO2
MgCl2·6H2O
Buffer solution (pH=10)
Calcined
MgO nanoparticles
Mg2(CO3)4(OH)2(H2O)4
(b)
1.00 μm

FIG. 1.

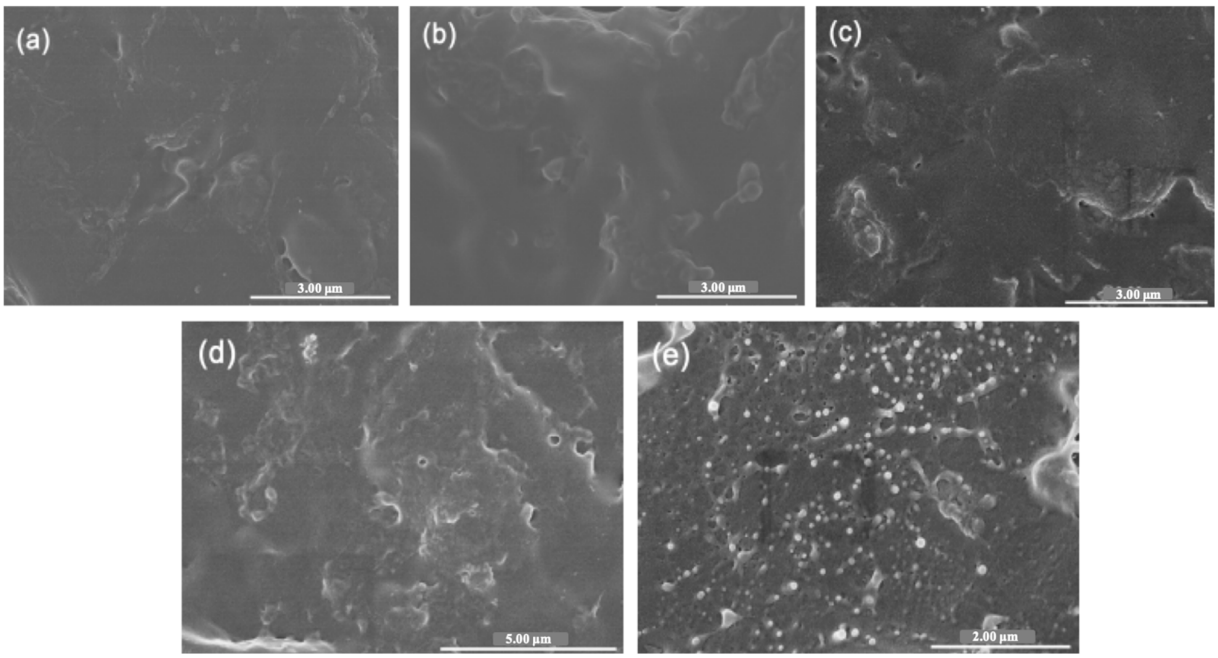
(a)
3.00 μm
(b)
3.00 μm
(c)
3.00 μm
(d)
5.00 μm
(e)
2.00 μm

FIG. 2.

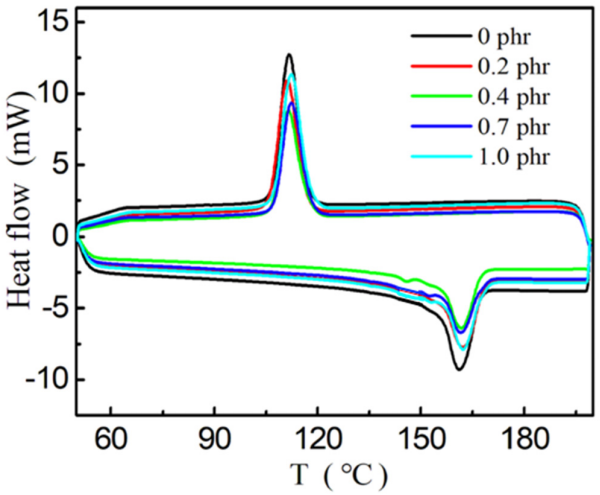
15
10
5
0
-5
-10
Heat flow (mW)
60
90
120
150
180
T (℃)
0 phr
0.2 phr
0.4 phr
0.7 phr
1.0 phr

FIG. 3.

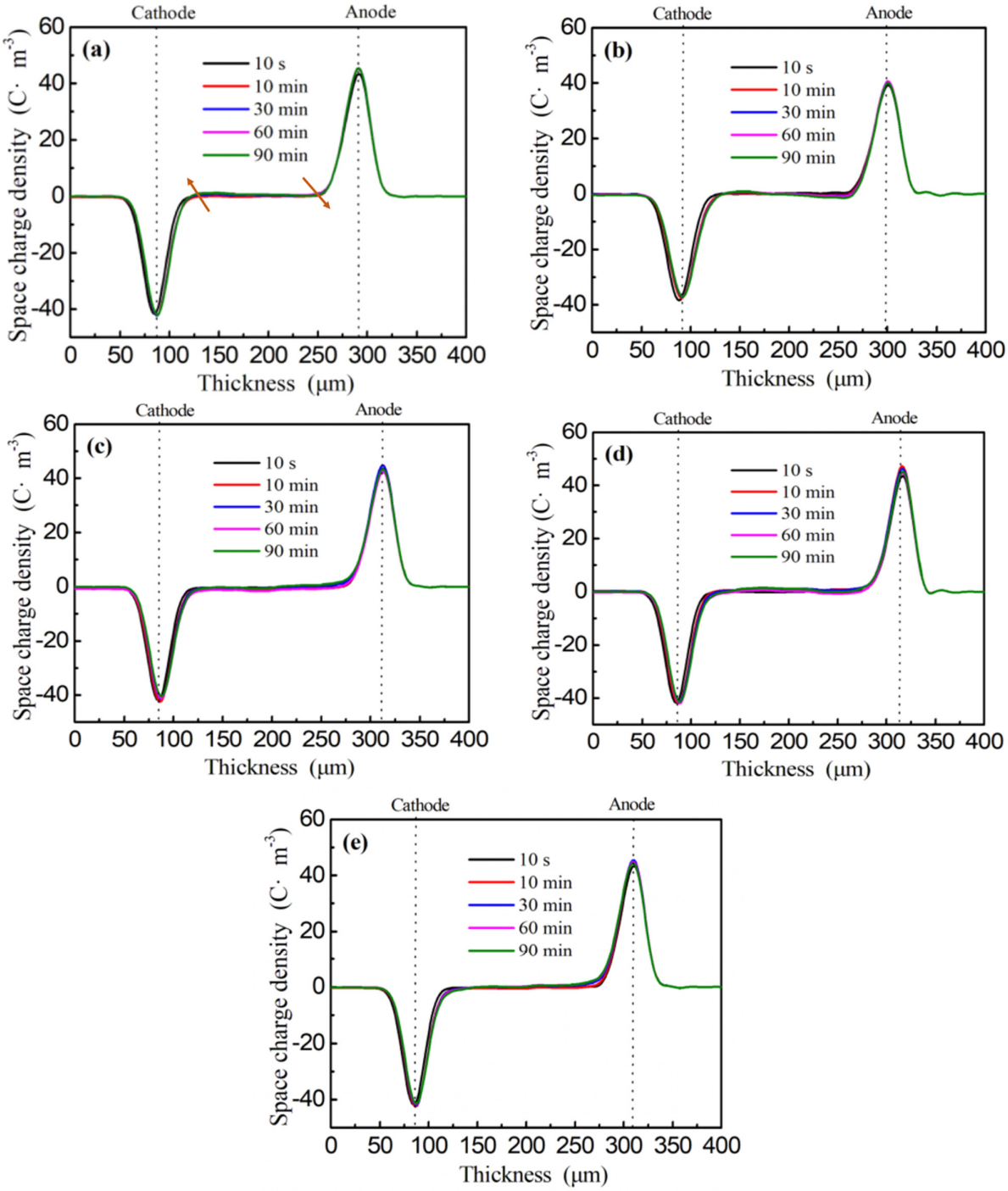
(a)
(b)
(c)
(d)
(e)
Cathode
Anode
10 s
10 min
30 min
60 min
90 min
Space charge density (C· m-3)
Thickness (μm)

FIG. 4.

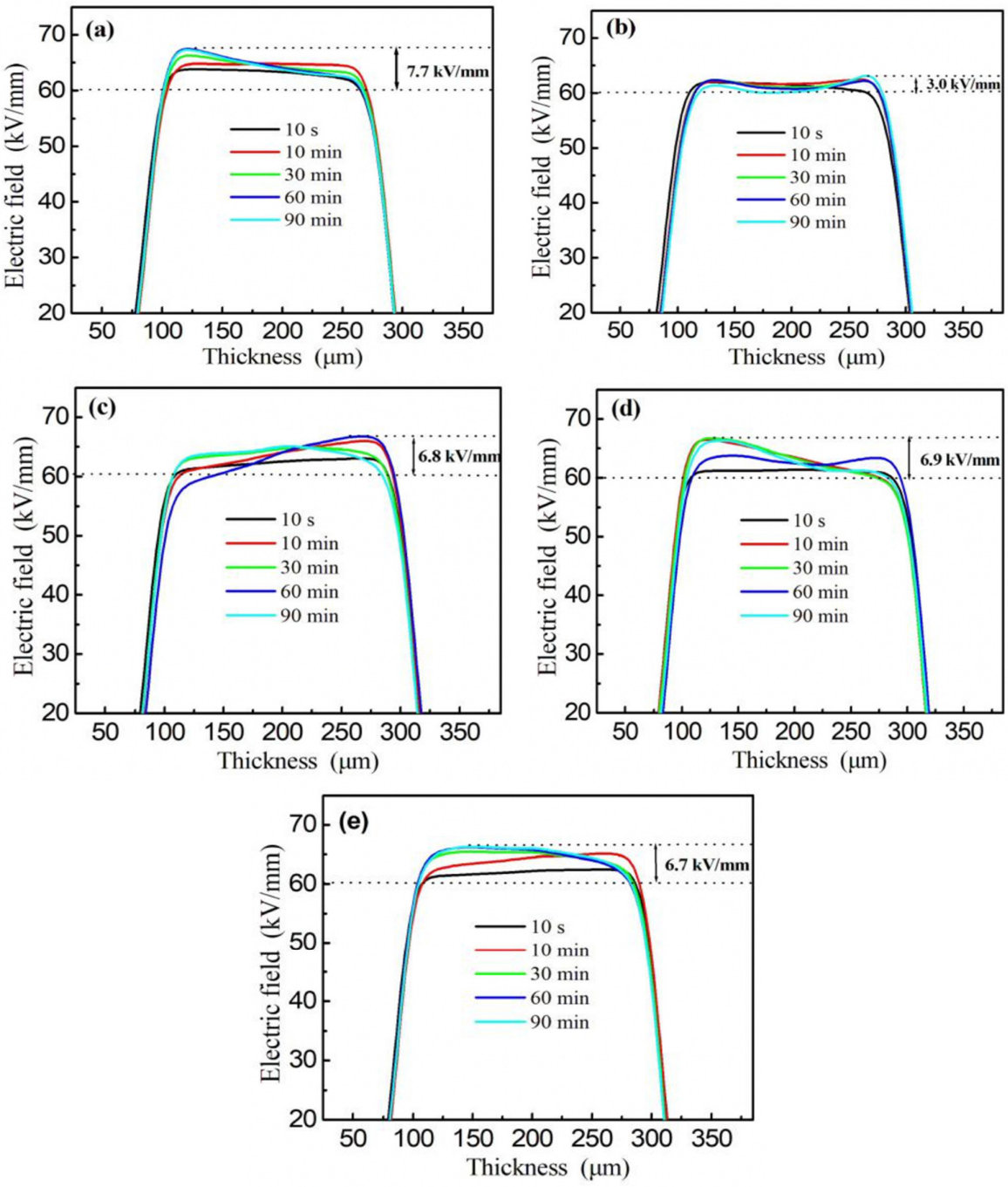
(a)
7.7 kV/mm
10 s
10 min
30 min
60 min
90 min
Electric field (kV/mm)
Thickness (μm)
(b)
3.0 kV/mm
(c)
6.8 kV/mm
(d)
6.9 kV/mm
(e)
6.7 kV/mm

FIG. 5.

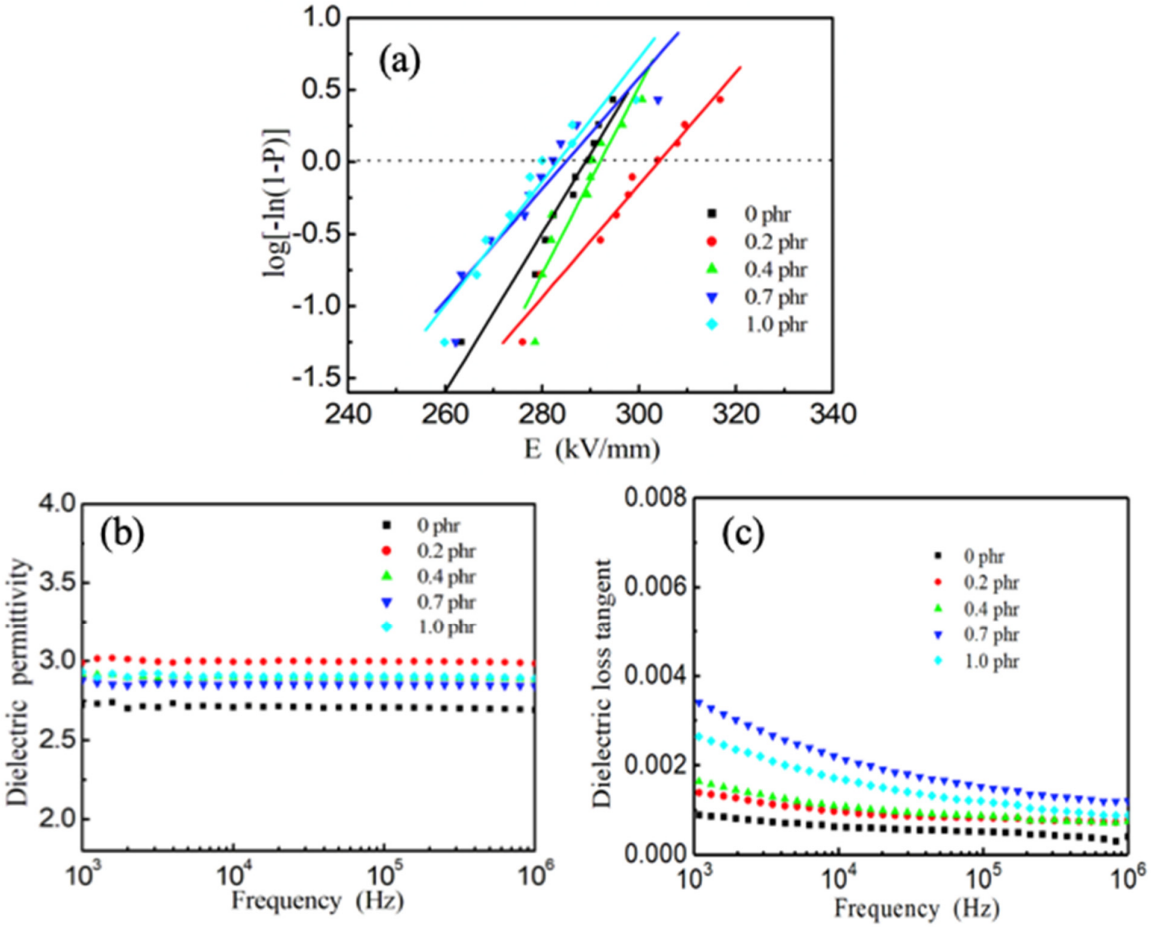
(a)
log[-ln(1-P)]
E (kV/mm)
0 phr
0.2 phr
0.4 phr
0.7 phr
1.0 phr
(b)
Dielectric permittivity
Frequency (Hz)
(c)
Dielectric loss tangent
Frequency (Hz)

FIG. 6.

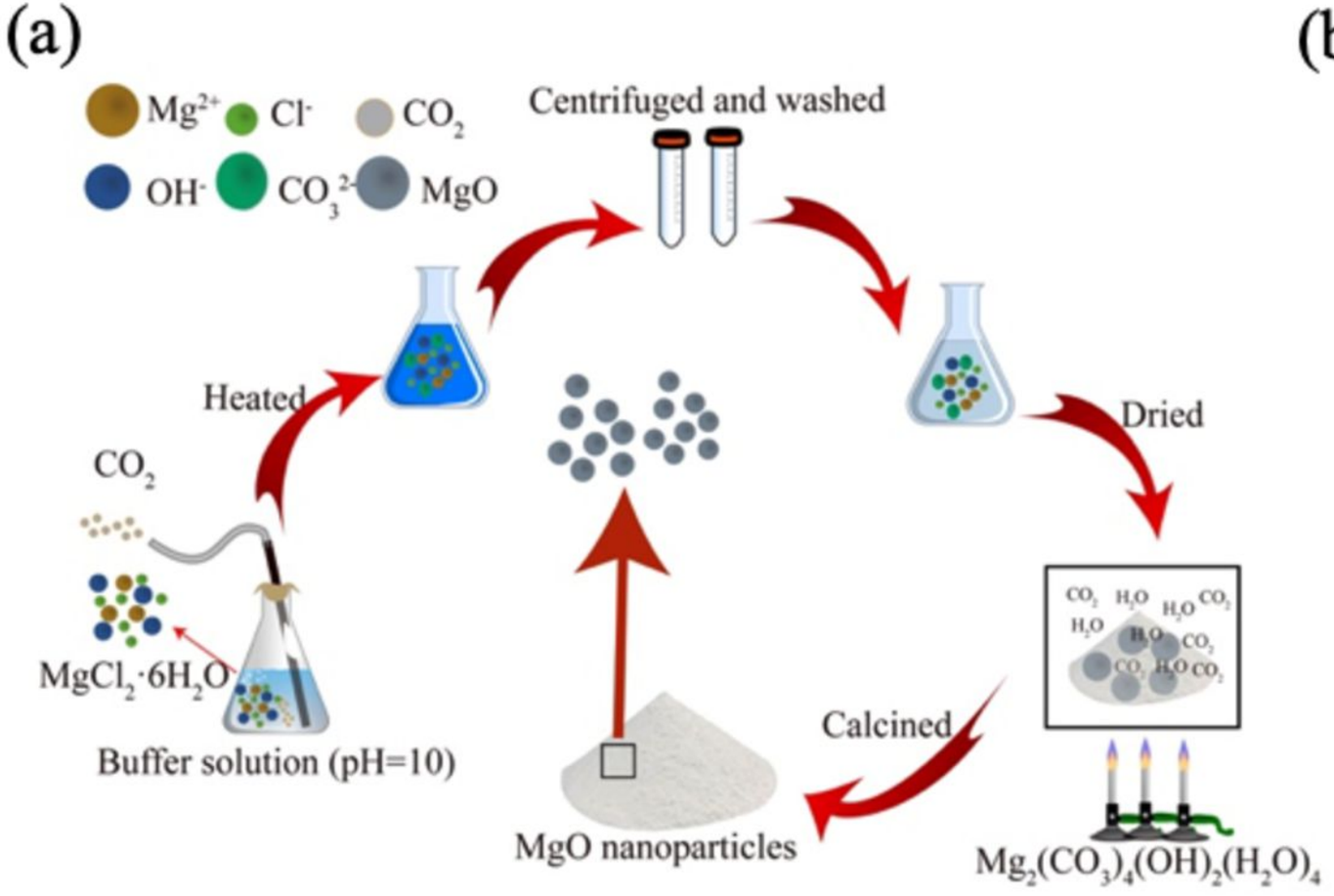
(a)
Mg^{2+}
Cl^-
CO_2
OH^-
CO_3^{2-}
MgO
Centrifuged and washed
Heated
Dried
CO_2
$MgCl_2 \cdot 6H_2O$
Buffer solution (pH=10)
Calcined
MgO nanoparticles
$Mg_2(CO_3)_4(OH)_2(H_2O)_4$

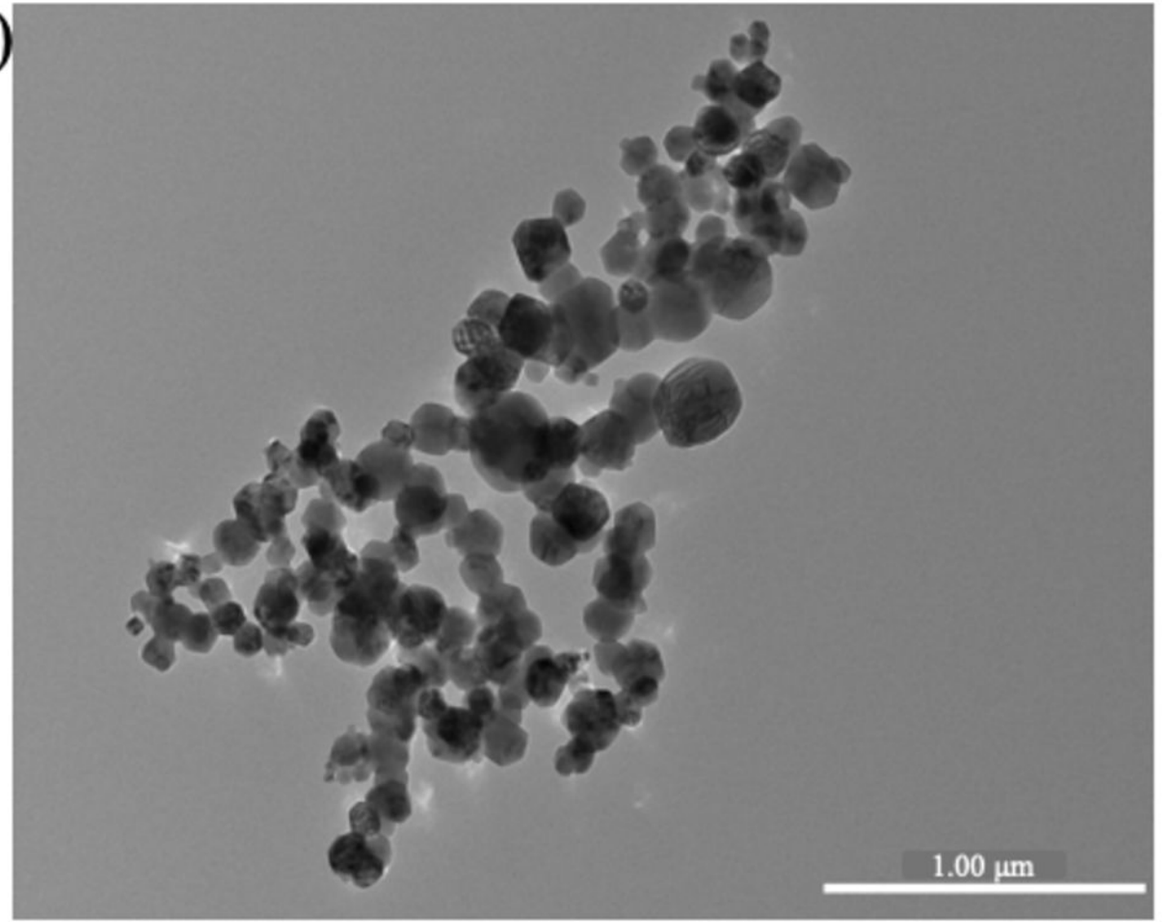
(b)
1.00 μm

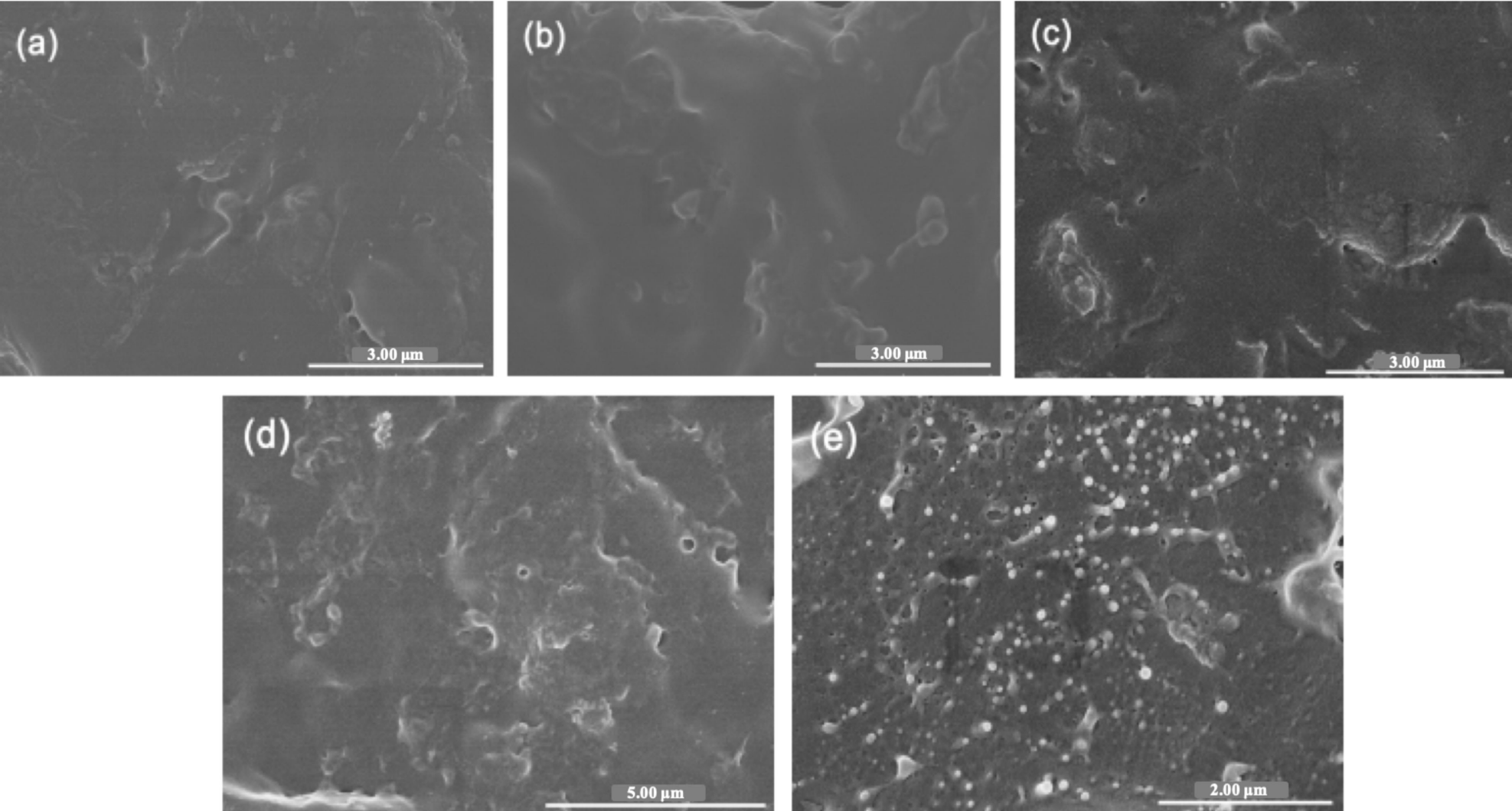
(a)
3.00 µm
(b)
3.00 µm
(c)
3.00 µm
(d)
5.00 µm
(e)
2.00 µm

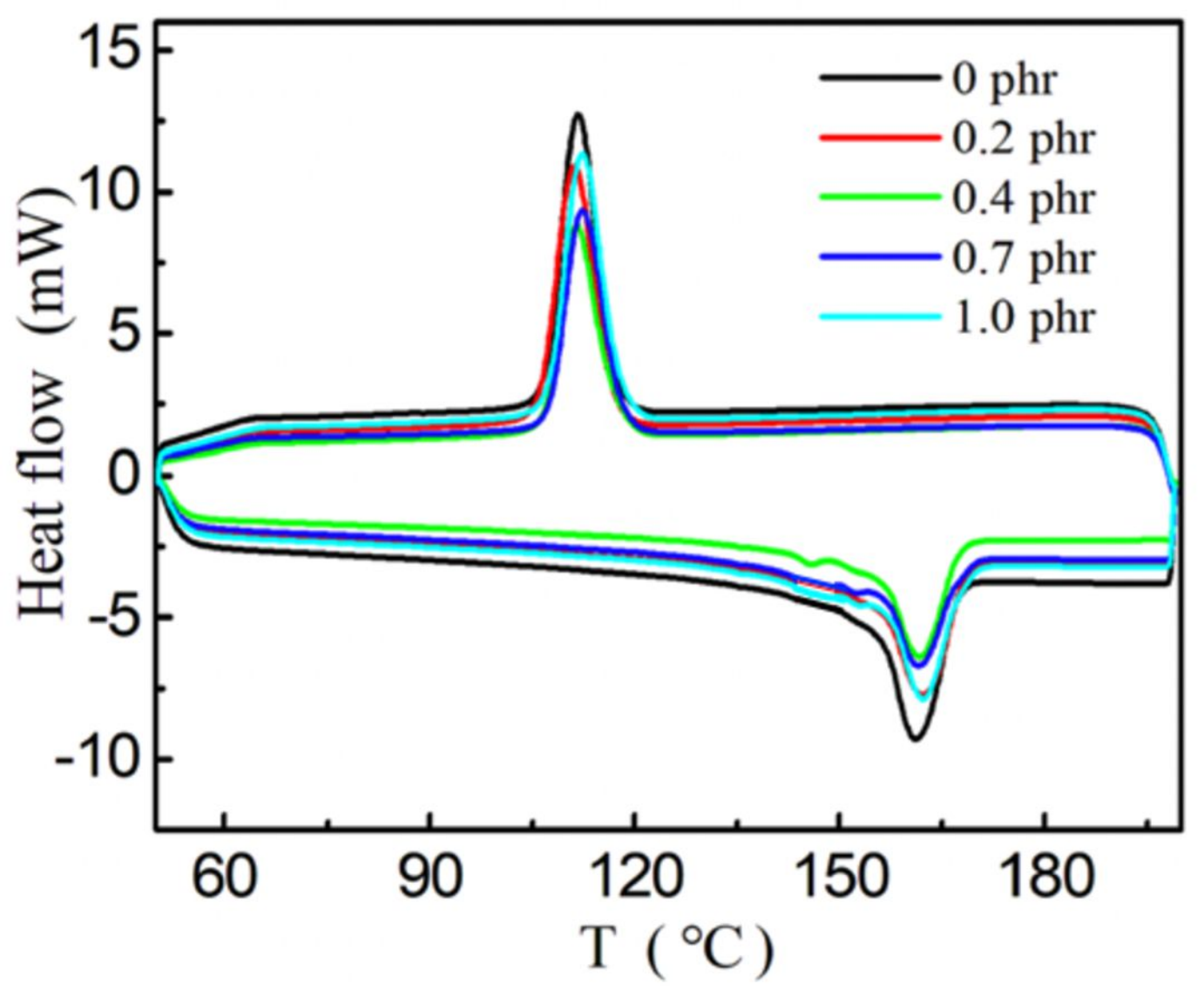
0 phr
0.2 phr
0.4 phr
0.7 phr
1.0 phr
Heat flow (mW)
15
10
5
0
-5
-10
60
90
120
150
180
T (°C)

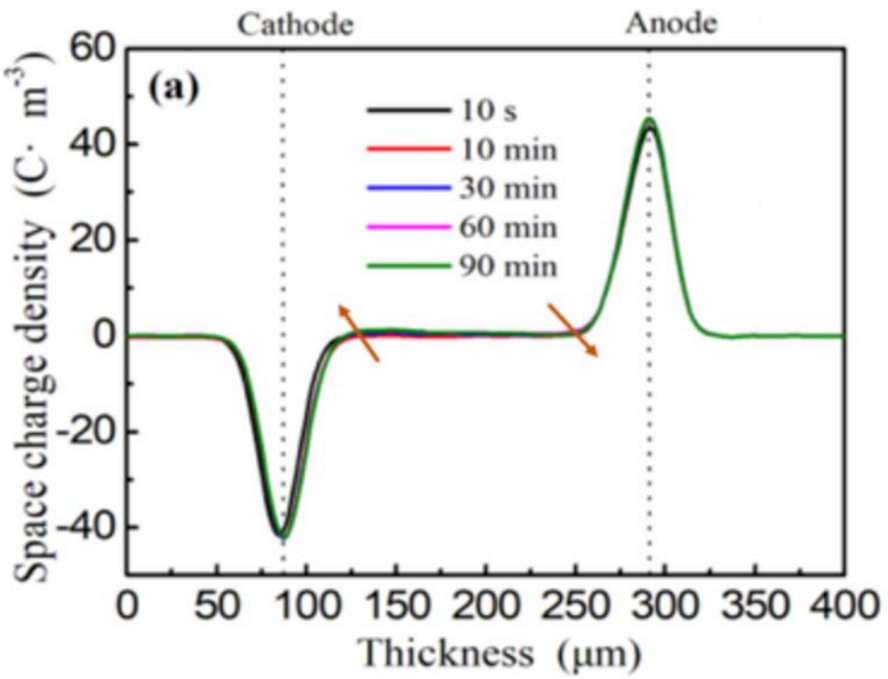
(a)
Cathode
Anode
10 s
10 min
30 min
60 min
90 min
Space charge density (C· m-3)
Thickness (μm)

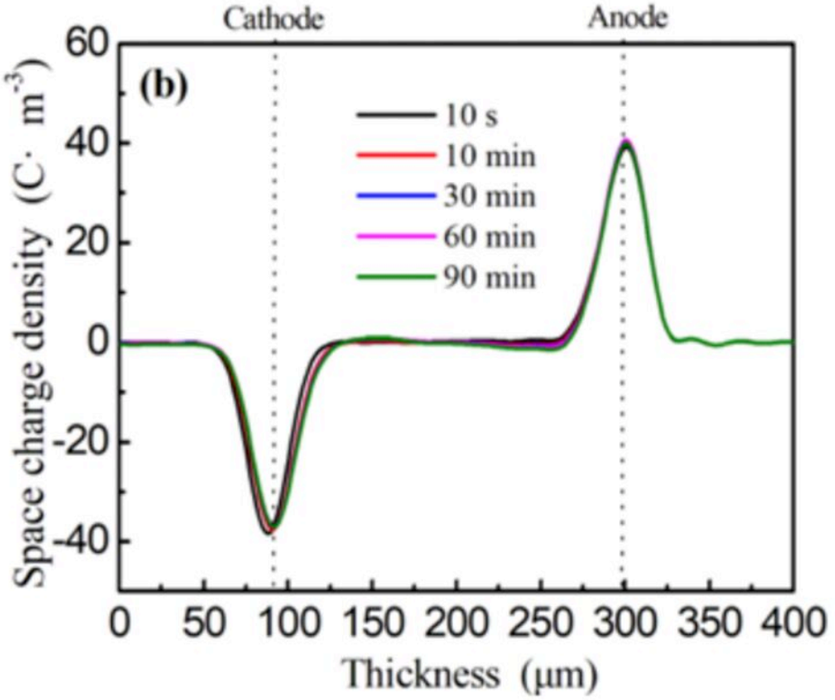
(b)
Cathode
Anode
10 s
10 min
30 min
60 min
90 min
Space charge density (C· m-3)
Thickness (μm)

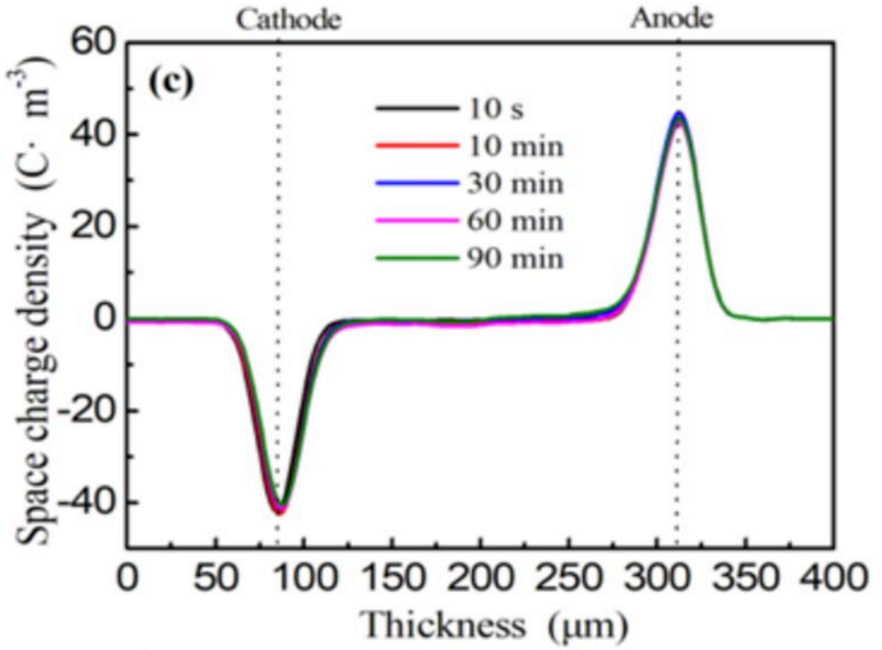
(c)
Cathode
Anode
10 s
10 min
30 min
60 min
90 min
Space charge density (C· m-3)
Thickness (μm)

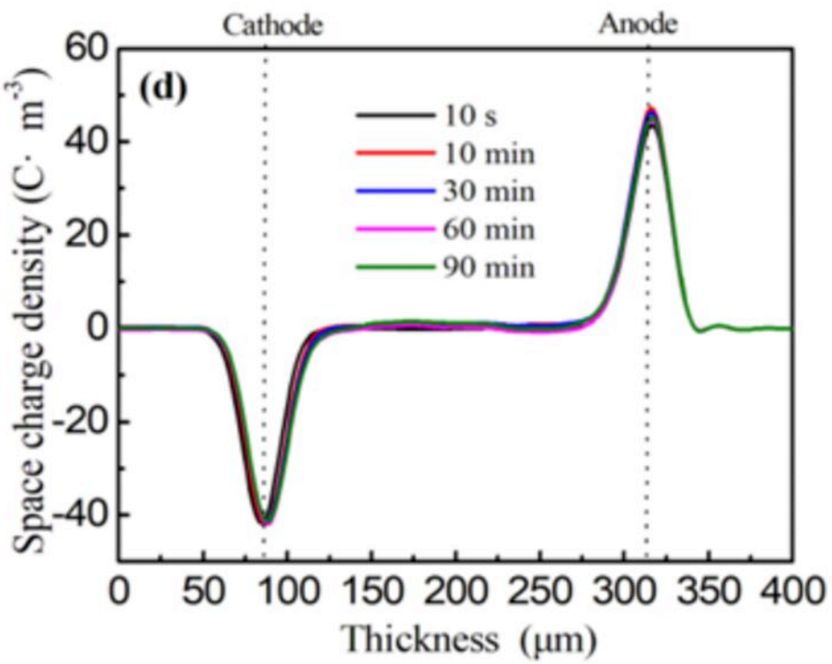
(d)
Cathode
Anode
10 s
10 min
30 min
60 min
90 min
Space charge density (C· m-3)
Thickness (μm)

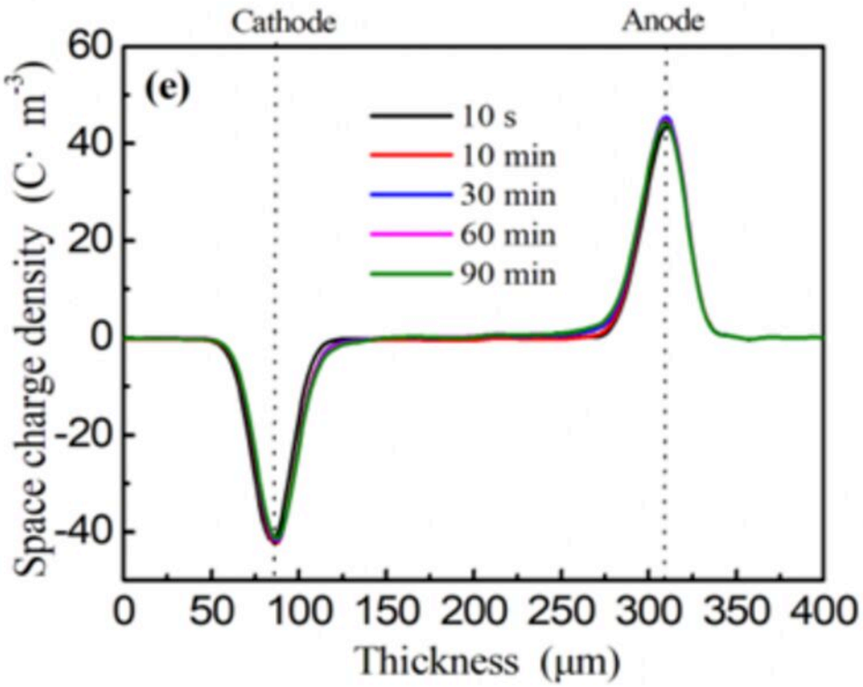
(e)
Cathode
Anode
10 s
10 min
30 min
60 min
90 min
Space charge density (C· m-3)
Thickness (μm)

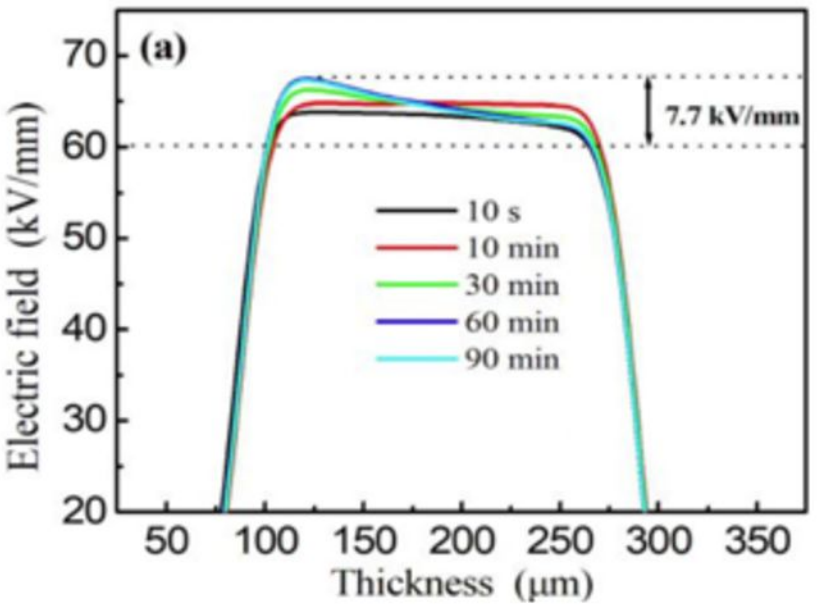
(a)
7.7 kV/mm
10 s
10 min
30 min
60 min
90 min
Electric field (kV/mm)
Thickness (μm)

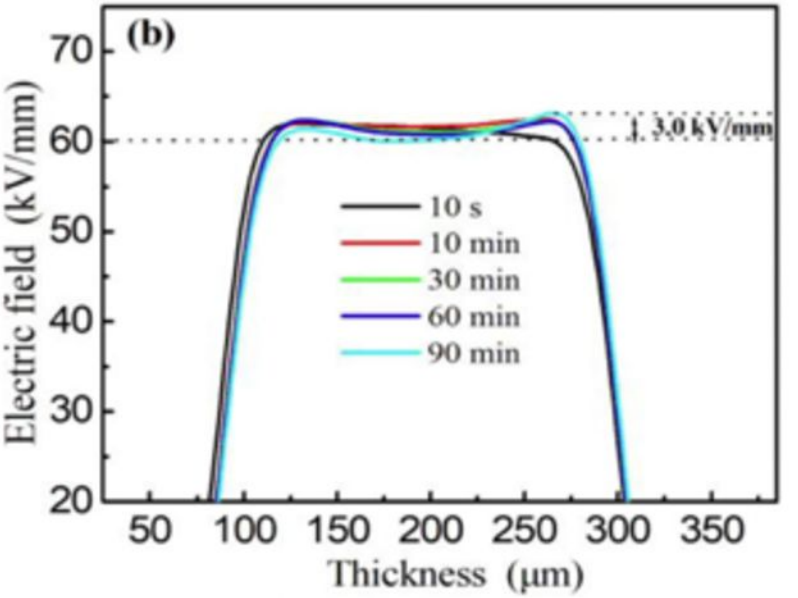
(b)
10 s
10 min
30 min
60 min
90 min
Electric field (kV/mm)
Thickness (μm)

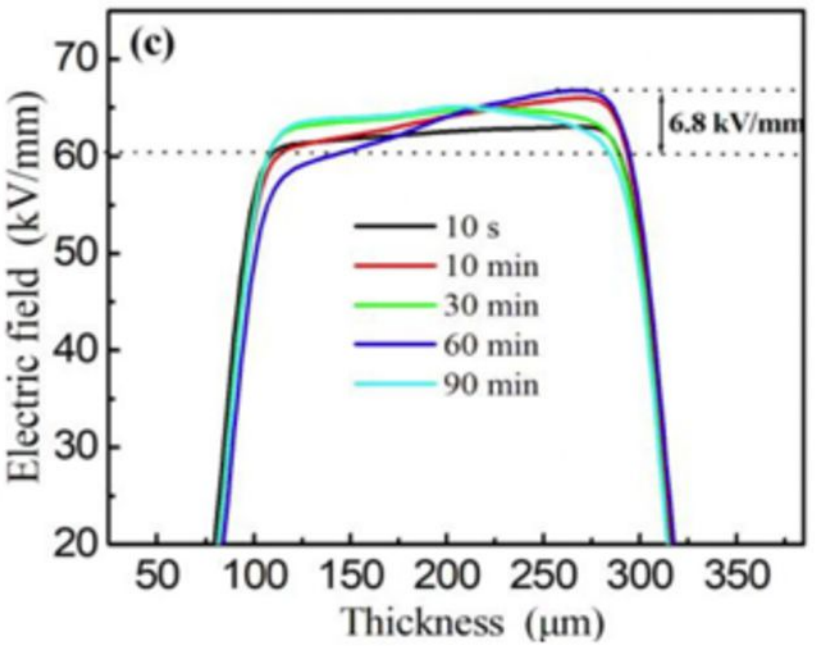
(c)
6.8 kV/mm
10 s
10 min
30 min
60 min
90 min
Electric field (kV/mm)
Thickness (μm)

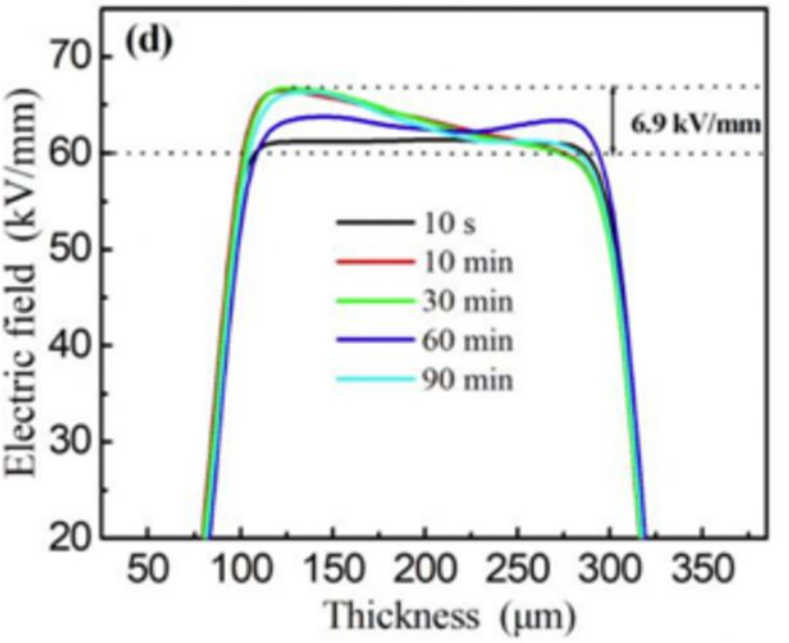
(d)
6.9 kV/mm
10 s
10 min
30 min
60 min
90 min
Electric field (kV/mm)
Thickness (μm)

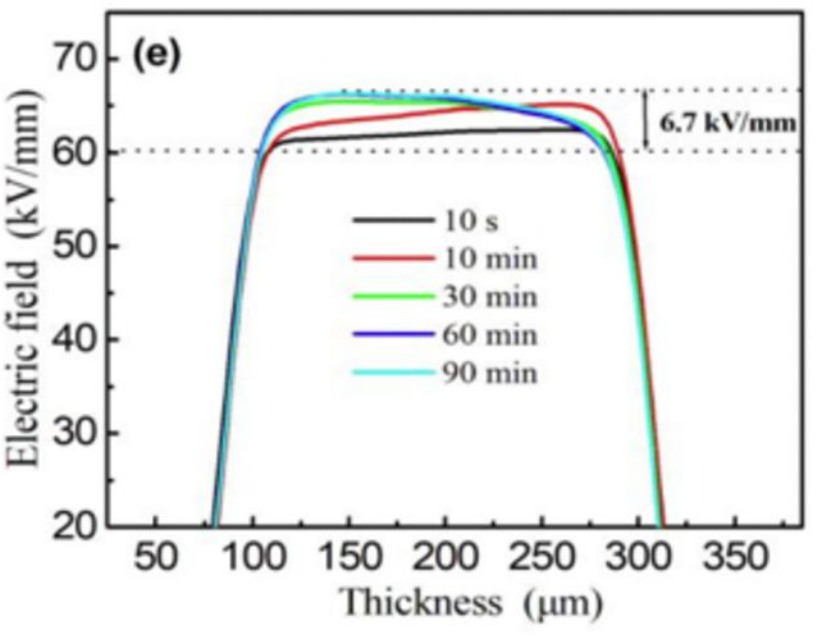
(e)
6.7 kV/mm
10 s
10 min
30 min
60 min
90 min
Electric field (kV/mm)
Thickness (μm)

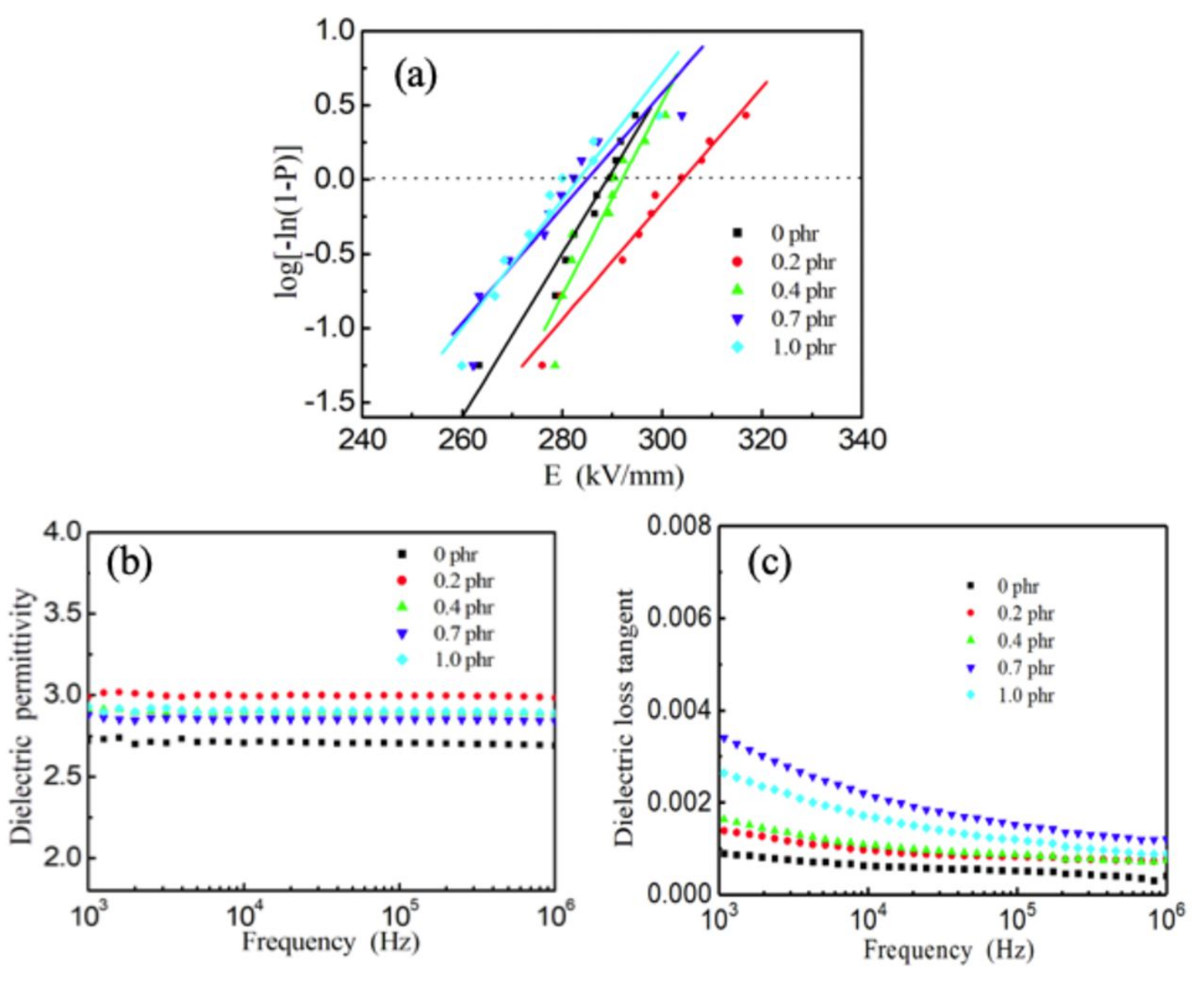
(a)
log[-ln(1-P)]
E (kV/mm)
0 phr
0.2 phr
0.4 phr
0.7 phr
1.0 phr
(b)
Dielectric permittivity
Frequency (Hz)
(c)
Dielectric loss tangent
Frequency (Hz)